Chemical Geology 655 (2024) 122083

Contents lists available at ScienceDirect

Chemical Geology

journal homepage: www.elsevier.com/locate/chemgeo

Microscale heterogeneity of phosphorus species associated with secondary mineral phases in the B horizons of two boreal Podzols

J.R. Marius Tuyishime [a,b,c], Tove Florén [a], Camille Rivard [d,e], Jon Petter Gustafsson [a,*]

[a] Department of Soil and Environment, Swedish University of Agricultural Sciences, P.O. Box 7014, Uppsala SE-75007, Sweden
[b] Department of Biology, Lund University, Ekologihuset, Sölvegatan 37, Lund 223 62, Sweden
[c] MAX IV Laboratory, P.O. Box 118, Lund 221 00, Sweden
[d] Beamline LUCIA, Synchrotron SOLEIL, L'Orme des Merisiers, Saint Aubin BP 48, Gif-sur-Yvette Cedex 91192, France
[e] TRANSFORM, INRAE, Nantes 44316, France

ARTICLE INFO

Editor: Oleg Pokrovsky

Keywords:
P spots
µ-XANES
µ-XRF mapping
B horizon
Imogolite-type materials

ABSTRACT

Poorly crystalline Al and Fe minerals have high sorption capacities for phosphate anions. However, there is still uncertainty about the molecular-level distribution of phosphorus (P) species between Al and Fe mineral phases, which can be relevant for bioavailability. The present study employed synchrotron X-ray microscopic techniques to distinguish between Al- and Fe-associated P phases in two Podzol B horizons (Flakaliden and Skogaby). First, P species were clustered into major groups depending on the main element association (Al-P, Fe-P, Ca-P + organic P) according to the color of P-containing spots in the tricolor µ-XRF quantitative maps that combined P, Al, and Fe fluorescence intensities. Second, the results were analyzed using quantitative linear combination fitting (LCF) of the P K-edge µ-XANES spectra. Third, in cases when the results diverged, a careful visual comparison between the diagnostic features of the XANES spectra of the samples and the reference standards was made. In 45 of 54 investigated spots, the color method and XANES-LCF produced consistent results. In 2 spots where the results were inconsistent, the diagnostic features of the XANES spectra agreed with the color method but not with XANES-LCF. In 39 of the 47 spots where the major P phase could be identified, Al-P was found to predominate. Ca-P was the major phase in 5 spots, Fe-P in 2, and organic P in 1. Most of the Al-P probably consisted of PO_4 adsorbed to imogolite-type materials (ITM), as evidenced by oxalate extraction and Fourier Transform Infrared (FTIR) spectroscopy, although at Skogaby, adsorbed organic P may have played an important additional role. Overall, the P speciation showed substantial spatial heterogeneity, particularly in the upper B horizon of the Skogaby soil and in the lower B horizon of the Flakaliden soil. In conclusion, Al-P, particularly ITM-adsorbed PO_4, is the main P phase in the B horizons of the studied Podzols, which may have implications for bioavailability as ITM is more easily dissolved than Fe oxides. Also, the combination of XANES-LCF, colors of the µ-XRF maps, and diagnostic features of the XANES spectra led to robust estimates of the major P phases in soil microsites.

1. Introduction

Phosphorus (P) species sorbed onto surface-reactive, short-range-ordered Al and Fe mineral phases in spodic B horizons constitute the largest P reservoir in boreal forest soils (Tuyishime et al., 2022; Wood et al., 1984). These mineral phases comprise mainly imogolite-type materials (ITM: proto-imogolite and well-developed imogolite) and ferrihydrite (Buurman and van Reeuwijk, 1984; Gustafsson et al., 1995; Sauer et al., 2007).

ITM and ferrihydrite form as a result of podzolization when organic acids from acidic surface soil horizons carry Fe^{3+} and Al^{3+} down to the B horizons, where poorly crystalline mineral phases are formed (Gustafsson et al., 1995; Lundström et al., 2000; Sauer et al., 2007). They possess a strong affinity for anions, partly due to their high point-of-zero charge; thus, dissolved P is sorbed onto their positively charged surface groups (Parfitt, 1979; Parfitt, 1989). Therefore, the poorly crystalline Al and Fe phases serve as geochemical buffers that prevent the loss of dissolved P (which includes both inorganic and organic forms) against leaching (Anderson et al., 1974; Borggaard et al., 2004; Wood et al., 1984). On the other hand, the continuous accumulation of ITM and Fe

---

* Corresponding author.
E-mail address: jon-petter.gustafsson@slu.se (J.P. Gustafsson).

https://doi.org/10.1016/j.chemgeo.2024.122083
Received 21 December 2023; Received in revised form 4 April 2024; Accepted 5 April 2024

oxides during podzolization results in secondary P build-up in the subsoil (Borggaard et al., 1990; Wood et al., 1984). This process gradually leads to “sink-driven” P-limiting conditions in the forest ecosystem, i.e., P limitation through adsorption or precipitation with Al and Fe precipitates (Vitousek et al., 2010).

Plants can take up PO_4 adsorbed to Al and Fe through strategies such as changes in the root architecture and excretion of organic acids by soil microorganisms, including mycorrhizal fungi (Doydora et al., 2020; Lang et al., 2017; Richardson and Simpson, 2011; Schreider et al., 2022). The extent to which this happens is, however, not clear, and available literature evidence appears contradictory. In a mesocosm experiment on a forest subsoil, Klotzbücher et al. (2020) found that beech was not able to acquire P from goethite mineral surfaces. On the other hand, Amadou et al. (2022) observed substantial uptake to ryegrass of P that had been adsorbed to goethite and gibbsite as PO_4 and organic P forms. For soils in which a considerable part of the soil P consists of adsorbed inorganic PO_4, it seems likely that plant uptake of P is related to the ratio of PO_4 to Fe and Al on the oxide surfaces, which reflects the P availability in the soil (Schreider et al., 2022; Tuyishime et al., 2022). Hence, the ecological and environmental relevance of Al-P and Fe-P could be better understood if these P phases could be accurately distinguished.

The acid oxalate extraction method has been commonly used to estimate the P concentration associated with Al and Fe mineral surfaces but cannot differentiate between these two phases (Hesterberg, 2010). Instead, P K-edge X-ray absorption near edge structure (XANES) spectroscopy can be applied to determine more accurately P speciation in the bulk soil (“bulk” P K-edge XANES) (Beauchemin et al., 2003; Eriksson et al., 2016; Hesterberg et al., 2017; Prietzel et al., 2016a; Prietzel et al., 2022; Rivard et al., 2016; Tuyishime et al., 2022). However, due to the spatial heterogeneity of the soil, the soil medium consists of highly diverse low-P and high-P microsites, which also differ greatly in the P speciation (Adediran et al., 2022; Hesterberg et al., 2011; Rivard et al., 2016; van der Bom et al., 2022). Thus, results obtained using the bulk XANES method alone will only represent a weighted average composition of all individual P-containing species in the analyzed sample, with the possibility of missing minor, but reactive, phases. The microscale heterogeneity of the soil can be resolved by analyzing the elemental composition of individual microsites on a microscopic X-ray fluorescence (μ-XRF) map in combination with μ-XANES spectroscopy on selected spots (Hesterberg et al., 2017; Rivard et al., 2016; Vogel et al., 2021; Yamaguchi et al., 2021).

Recently, the vertical and spatial distribution of P-containing species in forest soils from the boreal climate were studied using synchrotron-based X-ray microspectroscopy (Adediran et al., 2020; Tuyishime et al., 2022). At the micrometer scale, P speciation was performed by analyzing P K-edge μ-XANES spectra for spots selected from μ-XRF maps. However, μ-XANES spectra often appear slightly distorted due to, e.g., the presence of spots that are highly concentrated in P (Adediran et al., 2022), sample topography and thickness variations in thin sections of the analyzed sample. Furthermore, beam defocusing over parts of the energy range may be an issue in certain setups (Hesterberg et al., 2017). This makes common data treatment techniques, such as linear combination fitting (LCF), more challenging and prone to greater uncertainty.

The present study aims to investigate the extent to which adsorbed P species are associated with Al and Fe phases in two spodic B horizons, and whether the microscale distribution of P-containing species between secondary Al and Fe mineral phases in two spodic horizons can be better understood by combining information from μ-XRF and μ-XANES. Hence in addition to using LCF, we focused on the colors of the selected P-rich spots from μ-XRF maps on the spatial distribution of P, Al, and Fe and on qualitative analysis of μ-XANES spectral shapes and characteristics.

2. Materials and methods

2.1. Site description

This study used soil samples from the Flakaliden and Skogaby sites in Sweden. Both these forests consist of a Norway spruce (*Picea abies* L. Karst) stand planted on soils developed from siliceous glacial till deposits (Tuyishime et al., 2022).

Flakaliden (64°07′N, 19°27′E) has a boreal climate with long cold winters. The average mean temperature (MAT) and precipitation (MAP) are 1 °C and 600 mm, respectively. The current stand is approximately 60 years old and was planted with locally produced 4-year-old seedlings after clear-cutting (Albaugh et al., 2009; Bergh et al., 1999). This site has been studied extensively to test the effects of fertilization and irrigation on tree growth and carbon cycling; the experiments started in 1986 (Bergh et al., 1999).

The Skogaby (56°33′N, 13°13′E) forest is in the hemiboreal climatic zone. The MAT and MAP are 7.6 °C and 1100 mm, respectively. The current Norway spruce stand was planted in 1966, replacing a 53-year-old Scots pine stand (Simonsson et al., 2015). The site has long been exposed to atmospheric sulfur (S) and nitrogen (N) deposition although the deposition has been declining since the 1990s thanks to stricter emission controls and reduced industrial pollution (Bergholm et al., 2003). Previous studies at the Skogaby forest focused on the effects of nutrient deposition and status on tree vitality and growth (Nilsson and Wiklund, 1995; Simonsson et al., 2015).

Considering the entire B horizon, Flakaliden had higher pH(H_2O), and higher concentrations of P, Al, and Fe than Skogaby. Details of soil sampling and analyses of soil properties and chemically extractable P are described in Tuyishime et al. (2022). The properties of the studied soil samples are summarized in Table S1.

At both sites, the soils were classified as Albic Podzols (IUSS Working Group, 2014) but are generally characterized by slightly different degrees of Al and Fe accumulation from the overlying E horizons (Tuyishime et al., 2022). While oxalate-extractable Al (Al_{ox}) was higher in the Flakaliden B horizon samples, oxalate-extractable Fe (Fe_{ox}) was similar in both soils. The ratios of pyrophosphate- to oxalate-extractable Fe and Al were higher in the Skogaby samples, reflecting the higher organic C content when samples from similar depths are compared. The total P concentrations in the 20–30 cm and 40–50 cm Flakaliden samples were 30 mmol kg^{-1} and 16.5 mmol kg^{-1}, respectively, compared to 3.8 and 10 mmol kg^{-1}, respectively, in the 10–20 cm and 30–40 cm samples from Skogaby (Table S1). On average, according to bulk P K-edge XANES, of the total P in the B horizon at both sites, 60–67% was PO_4 adsorbed to or precipitated with Al, and 22–30% was PO_4 adsorbed to or precipitated with Fe (Tuyishime et al., 2022).

At both sites, the mineralogy of the fine earth is dominated by quartz, followed by plagioclase and K-feldspar (Casetou-Gustafson et al., 2018, 2019, 2020; Simonsson et al., 2015, 2016). According to X-ray Powder Diffraction (XRPD), the fraction of poorly crystalline Al minerals in the fine earth of the B horizons of the two sites varied between 4 and 8%, whereas amorphous Fe minerals ranged between 0.1 and 2% (Simonsson et al., 2015; Tuyishime et al., 2022).

2.2. Identification of imogolite-type materials

Fourier Transform Infrared Spectroscopy (FTIR) was used to investigate to what extent ITM could be identified as an important secondary Al phase in the soils. Four samples were chosen, representing the upper B horizons (Flakaliden 30–40 cm, Skogaby 20–30 cm) and the middle part of the B horizons (Flakaliden 40–50 cm, Skogaby 30–40 cm). The acid-dispersible clay fraction (<0.5 μm) of the samples was isolated through acid dispersion, ultrasonication, centrifugation, and lyophilization, according to the method of Farmer et al. (1980). FTIR spectra of the lyophilized samples were recorded at room temperature for 13 mm KBr discs on a Pelkin-Elmer Spectrum 100 in transmittance mode, with

16 scans between wavenumbers 400 cm^{-1} to 4000 cm^{-1}. For the soil sample (Skogaby 30–40 cm) where ITM features could not be detected, the sample was heated to 350 °C. The FTIR spectrum was again recorded, and a difference spectrum calculated (c.f. Gustafsson et al., 1999).

2.3. Phosphorus speciation in microsites

The analyzed soil samples (20–30 cm and 40–50 cm from Flakaliden B horizon and 10–20 cm and 30–40 cm from Skogaby B horizon) were prepared as petrographic thin sections (30 μm thick) by embedding the soil in high-purity epoxy resin and mounted on glass slides at the T.S. Lab & Geoservices snc, Cascina, Italy.

The experiment combining μ-XRF for elemental colocalization mapping and μ-XANES techniques was performed at the French national synchrotron research facility SOLEIL in its micro-focused LUCIA beamline (Vantelon et al., 2016). The Si(111) double crystal monochromator energy was calibrated to the maximum of the first derivative of $AlPO_4$ at 2154.8 eV.

Two-dimensional (2D) maps (700 × 700 μm) were acquired by focusing a 2.8 × 2.8 μm X-ray beam on soil samples (thin sections) to collect P, Al, Si, and Fe fluorescence signal. To obtain high-quality data on P compounds, the scan was carried out at 2.6 keV, an energy slightly above the P K-edge energy using a dwell time of 0.3 s and a step size of 3 × 3 μm. Thus, Fe maps were obtained using its L_3-edge peak centered at 707 eV.

After elemental mapping, P K-edge μ-XANES was collected in several microsites (Pt), selected from microscale P distribution maps. The spectra were recorded in fluorescence-yield mode using a Si-drift detector with energy step of 2 eV between 2100 and 2139 eV, 1 eV between 2139 and 2146 eV, 0.2 eV between 2146 and 2160 eV, 0.3 eV between 2160 and 2190 eV, and 5 eV between 2190 and 2322 eV. For each map, between 5 and 20 Pts were selected. From each selected Pt, two μ-XANES scans were collected.

2.4. Data analysis

μ-XRF spectra for each element were batch-fitted at each pixel using Python Multichannel Analyzer (PyMCA, Solé et al., 2007) to extract P, Al, and Fe elemental maps and data were corrected from the detector deadtime value. Using Fiji (ImageJ-win64) software (Chandez and Montarou, 2010), for a given element, the same contrast scale (in black and white colors) was applied across all maps to ensure correct intensity comparison. The resulting maps were then combined to create RGB composite μ-XRF maps of P, Al, and Fe.

A color picker tool in the Affinity Designer software (Serif Ltd., Nottingham, UK) was used to sample the color from processed RGB μ-XRF maps of P, Al, and Fe and to enlarge the features to present the color distribution of Pts in the microsites. The blue, green, and red colors in the RGB maps were assigned to Al, Fe, and P, respectively. Pink and yellow colors therefore indicate an association between P and Al, and between P and Fe, respectively. Other P-containing species e.g., organic P or P associated with Ca, will be red-colored.

Collected P K-edge μ-XANES scans of samples were merged, normalized, and then analyzed with linear combination fitting (LCF) using the Athena software (version 0.9.25) (Ravel, 2009; Ravel and Newville, 2005). The standards used in this study to fit XANES sample spectra consisted of soil organic P (Podzol Oe horizon sample from central Sweden, assumed to represent generic soil organic P), PO_4 adsorbed to ITM, PO_4 adsorbed to gibbsite, PO_4 adsorbed to amorphous $Al(OH)_3$, PO_4 adsorbed to ferrihydrite, PO_4 adsorbed to goethite, variscite, amorphous $AlPO_4$, strengite, amorphous $FePO_4$, apatite Taiba, hydroxyapatite, and brushite (Fig. 1). For additional details about the standards used, see Gustafsson et al. (2020). The LCF weights were renormalized to a sum of 1 and presented as percentages. The uncertainties of the weights, as presented in Tables 1 and 2, are those reported by Athena; these are the uncertainties of the LCF procedure itself, but do not include the uncertainties associated with energy calibration and normalization (Gustafsson et al., 2020).

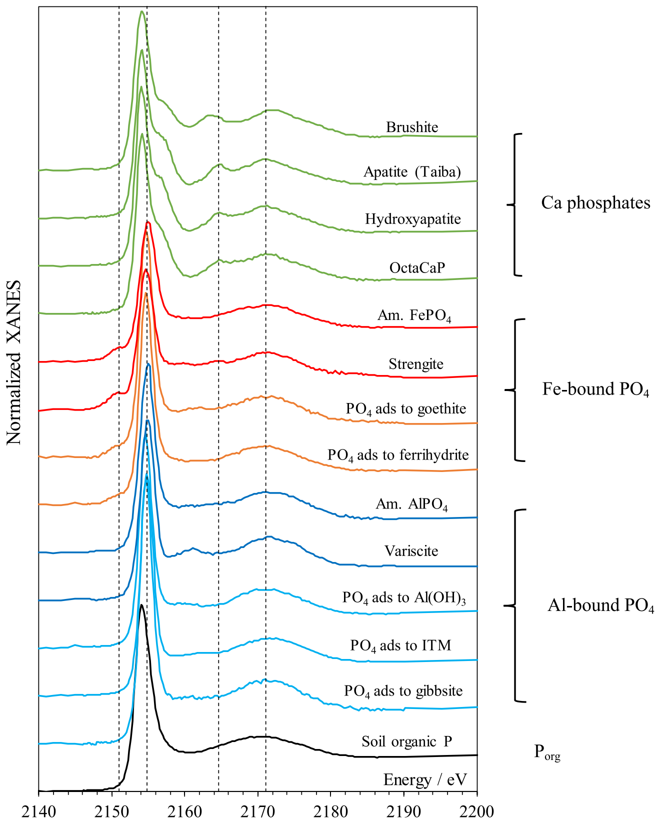

Fig. 1. X-ray absorption near-edge spectroscopy (XANES) spectra of 14 standards and standard groups of relevant P-containing species that were used in linear combination fitting. The dashed lines correspond to the pre-edge of Fe (III)-bound PO_4 phases (2151 eV), the white-line maximum energy of variscite (2154.8 eV), the first post-edge peak of hydroxyapatite (2164.6 eV), and the second post-edge peak of hydroxyapatite (2171.1 eV).

To determine the major P phase, the following procedure was used: if the XANES-LCF speciation was consistent with the μ-XRF color, the major P phase, as determined by XANES-LCF, was considered correct.

3. Results and discussion

3.1. Characterization of poorly ordered Al phases

The Flakaliden 40–50 cm sample had double peaks at 994 and 940 cm^{-1} and 592 and 567 cm^{-1} (Fig. 2), associated with Si – O vibrations. These features are the spectral fingerprint of well-ordered tubular imogolite (Gustafsson et al., 1995). The absorption bands at 432 cm^{-1} and 496 cm^{-1} are attributed to Al-OH and Si-O-Al vibrations, respectively, indicating the presence of proto-imogolite (Bishop et al., 2013; Farmer et al., 1977; Gustafsson et al., 1995).

In the two other samples, the presence of ITM was less evident due to the presence of other phases, such as organic matter and crystalline clays, which masked the ITM-specific features. The peaks at ~1720, 1695, 1416, 1289 and 815 cm^{-1} were attributed to carboxylates. The peaks between 1030 and 1130 cm^{-1} are typical for Si-O stretching vibrations of crystalline silicate clays. For Flakaliden 20–30 cm, the presence of a dioctrahedral layer silicate (probably illite) was evident by additional peaks at 915, 532 and 472 cm^{-1}, which is consistent with X-ray diffraction results for the same soil (Tuyishime et al., 2022). Further, a small amount of kaolinite was identified (3620 and 3698 cm^{-1}). Even so, for Flakaliden 20–30 cm the presence of ITM was indicated, although not conclusively, by peaks at 1000 cm^{-1} and 432 cm^{-1} (Si-O(H)

Table 1

Phosphorus speciation in the Flakaliden soil B horizon as evidenced from linear combination fitting (LCF) of μ-XANES spectra collected from 20 microsites at 20–30 cm and 10 microsites at 40–50 cm and determination of the major phase after consideration of LCF, colors, as well as main diagnostic features (see text). The fits are expressed as percentage contributions from selected P standards. "Undecided" means that the XANES-LCFs were of poor quality.

Soil	Pt no	P_{org}	Al-bound PO_4		Fe-bound PO_4		Ca-P	R-factor	Major phase
			Al-adsorbed	$AlPO_4$	Fe-adsorbed	$FePO_4$			
Flakaliden									
B 20–30	1		63.5 ± 4	28.0 ± 10		8.4 ± 7		0.006	Al-bound PO_4
	2		78.5 ± 4	12.0 ± 2	9.0 ± 5			0.003	Al-bound PO_4
	3						99.9 ± 12	0.07	Ca-phosphate
	4		100.0 ± 12					0.007	Al-bound PO_4
	5		58.1 ± 8		41.9 ± 8			0.009	Al-bound PO_4
	6		70.3 ± 4	5.5 ± 12		24.1 ± 9		0.01	Al-bound PO_4
	7		86.0 ± 7		13.7 ± 8			0.007	Al-bound PO_4
	8		65.2 ± 10		34.7 ± 7			0.005	Al-bound PO_4
	9		91.0 ± 7	3.3 ± 9	2.5 ± 7	3.0 ± 7		0.004	Al-bound PO_4
	10		11.0 ± 8	21.7 ± 10	56.5 ± 8	10.8 ± 8		0.008	Undecided
	11		85.4 ± 3	9.6 ± 1	4.8 ± 4			0.001	Al-bound PO_4
	12		100.0 ± 8					0.008	Al-bound PO_4
	13		89.9 ± 3	4.5		5.0 ± 6		0.004	Al-bound PO_4
	14		68.7 ± 4		17.7 ± 8	13.5 ± 1		0.007	Al-bound PO_4
	15		66.1 ± 19		34.0 ± 12			0.02	Al-bound PO_4
	16		84.5 ± 1	15.4 ± 2				0.003	Al-bound PO_4
	17		67.6 ± 6	1.0 ± 3	31.0 ± 8			0.006	Al-bound PO_4
	18	15.9 ± 4	84.0 ± 3					0.03	Al-bound PO_4
	19		84.0.6 ± 2	15.4				0.006	Al-bound PO_4
	20		85.0 ± 7	14.9				0.006	Al-bound PO_4
B 40–50	1		99.9 ± 29					0.03	Al-bound PO_4
	2		1.0 ± 8			98.8 ± 11		0.3	Undecided
	3		44.7 ± 3	12.0 ± 9		43.2		0.009	Al-bound PO_4
	4				n.d				Undecided
	5		57.9 ± 6	16.0 ± 16		25.6 ± 12		0.02	Al-bound PO_4
	6					13.3 ± 9	85.6 ± 67	0.2	Ca-phosphate
	7		73.5 ± 5	5.6 ± 13		20.8		0.009	Al-bound PO_4
	8		64.7 ± 7	27.7 ± 18	7.6 ± 13			0.02	Al-bound PO_4
	9		44.3 ± 9	9.6 ± 24		46.0 ± 18		0.05	Al-bound PO_4
	10		76.0 ± 15		24.0 ± 16			0.03	Al-bound PO_4

Table 2

Phosphorus speciation in the Skogaby soil B horizon as evidenced from linear combination fitting (LCF) of μ-XANES spectra collected from 12 microsites at 10–20 cm and 12 microsites at 30–40 cm and determination of the major phase after consideration of LCF, colors, as well as main diagnostic features (see text). The fits are expressed as percentage contributions from selected P standards. * on the Pt no Indicates the data when the color of Pts and XANES-LCF were not consistent. "Undecided" means that the XANES-LCF:s were of poor quality.

Soil	Pt no	P_{org}	Al-bound PO_4		Fe-bound PO_4		Ca-P	R-factor	Major phase
			Al-adsorbed	$AlPO_4$	Fe-adsorbed	$FePO_4$			
Skogaby									
	1	n.d							Undecided
B 10–20	2	17.0 ± 1	42 ± 3	10.0 ± 7		30.1 ± 5		0.005	Undecided
	3	42.8 ± 4			37.6 ± 2		19.6 ± 3	0.009	P_{org}
	4					43.8 ± 6	56.2 ± 14	0.09	Ca-phosphate
	5	5.5 ± 8			93.6 ± 18		0.7 ± 8	0.02	Undecided
	6*	14.9 ± 2	24.8 ± 3		43.9 ± 3		16.4 ± 2	0.001	Al-associated P
	7	31.2 ± 9			27.4 ± 5		41.4 ± 8	0.06	Ca-phosphate
	8	3.1	72.8 ± 13			24.2 ± 7		0.002	Al-bound PO_4
	9		98.7 ± 3	2.2 ± 3				0.007	Al-bound PO_4
	10		90.5 ± 2.5	9.5 ± 3				0.007	Al-bound PO_4
	11	16.2 ± 2	23.6 ± 8		60.2 ± 10			0.009	Fe-bound PO_4
	12	20.3 ± 2	23.8 ± 11		55.9 ± 12			0.01	Undecided
	13		47.7	18.6 ± 3	34.1 ± 6			0.002	Al-bound PO_4
B 30–40	1		51.0 ± 15	16.7 ± 13		31.5 ± 10		0.01	Al-bound PO_4
	2		97.2 ± 2	2.7 ± 2				0.005	Al-bound PO_4
	3		66.2	3.0 ± 9		29.8 ± 7		0.007	Al-bound PO_4
	4		70.5 ± 1			23.7 ± 1	5.8 ± 1	0.002	Al-bound PO_4
	5*		67.1 ± 9		19.8 ± 19	13.0 ± 0		0.01	Fe-associated P
	6		50.3 ± 29	19.9 ± 25		29.8 ± 1		0.05	Al-bound PO_4
	7		72 ± 3	11.1 ± 7		16.5		0.003	Al-bound PO_4
	8		89.6 ± 8		10.3 ± 7			0.009	Al-bound PO_4
	9		68.6 ± 5.5	4.2 ± 15		27 ± 11		0.02	Al-bound PO_4
	10					47.6 ± 26	52.5 ± 15	0.11	Ca-phosphate
	11		44.9 ± 4	19.1 ± 1	36 ± 3			0.001	Undecided
	12		62.3 ± 6	10.3	27.7			0.005	Al-bound PO_4

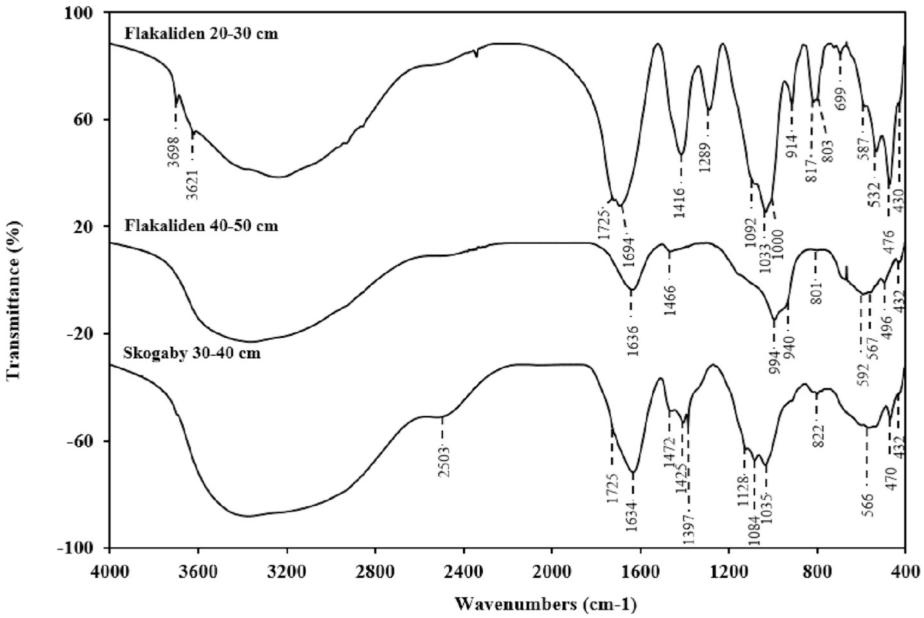

Fig. 2. Fourier Transform Infrared (FTIR) spectra for acid-dispersible clays recorded at room temperature from Flakaliden 20–30, Flakaliden 40–50, and Skogaby 30–40.

stretching of orthosilicate structures and Si-O bending of ITM, respectively). Unfortunately, the very low amount of acid-dispersible clay did not allow us to record a difference spectrum after heating to 350 °C. This was, however, possible for the Skogaby 30–40 cm sample, for which the presence of ITM was only indicated by a small 432 cm^{-1} band (Fig. 2). After heating, the difference spectrum showed more conclusive evidence for ITM by the appearance of a peak at 947 cm^{-1} and by the strengthening of the feature around 430 cm^{-1} (Fig. S1). Furthermore, the ratio of oxalate-extractable inorganic Al (Al_{ox} - Al_{py}) to Si_{ox} was between 2 and 2.7 in the studied B horizons (Table S1), consistent with ITM being the predominant oxalate-extractable Al mineral phase in the soils (Gustafsson et al., 1995; Parfitt, 1989; Tuyishime et al., 2022).

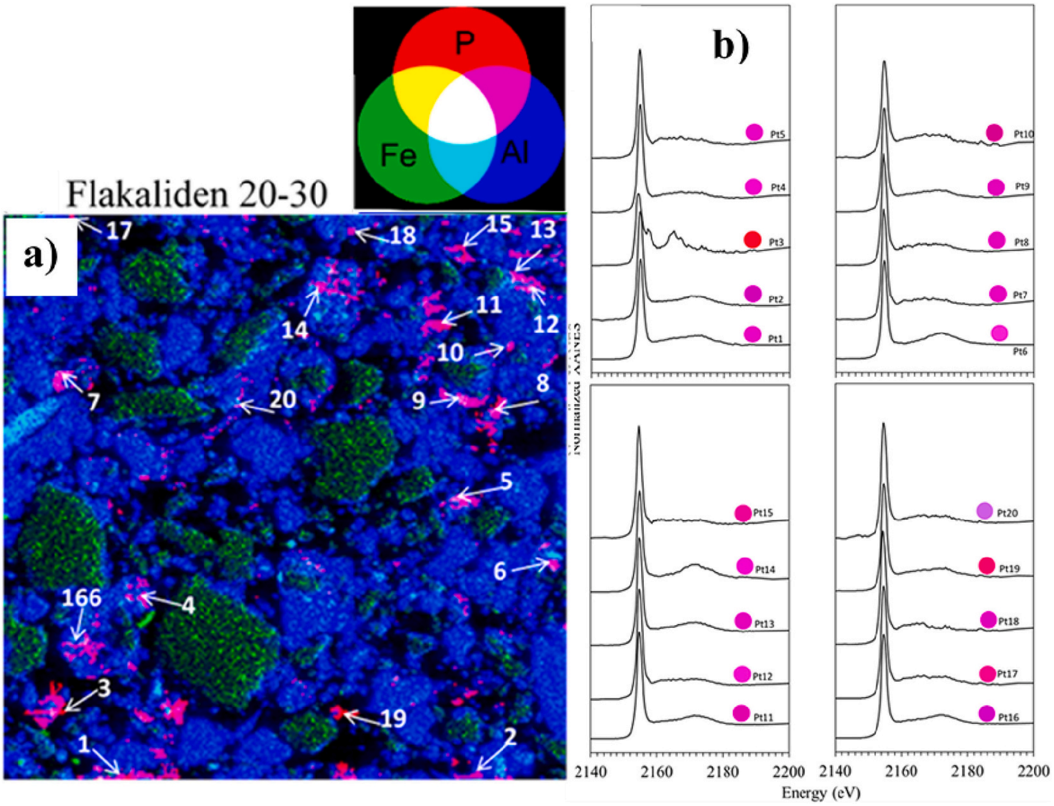

Fig. 3. RGB P-Fe-Al µ-XRF map (700 × 700 µm) of Flakaliden 20–30 cm (B horizon) and corresponding normalized P K-edge µ-XANES spectra of µ-Pts associated to their picked-up color.

3.2. *Phosphorus speciation in microsites*

Phosphorus species characterization in the Pts was carried using LCF of the µ-XANES data (Figs. S2-S5, example in Fig. S6, Tables 1–2). However, we also used the colors of the Pts from the RGB µ-XRF maps (Figs. 3–5), which provided information on the colocalization of P with other elements, and the main diagnostic features of the µ-XANES spectra, to more confidently determine the major P phases present in each Pt.

In 45 of 54 Pts, the RGB color agreed with the main phase as determined by XANES-LCF, showing a high degree of consistency between the two methods. For the other nine Pts, the mismatch may have been due, for example, to poor spectral quality. In situations when XANES-LCF and the µ-XRF colors disagreed, the spectral XANES features were investigated in more detail to get additional evidence. For Pt no. 6 of Skogaby 10–20 cm, the color was pink (Fig. 4), suggesting Al-associated P, while the LCF showed a predominance of Fe-bound PO_4 species (Table 2). However, inspection of the XANES spectrum could not reveal any evidence of a pre-edge feature typical for Fe phosphates or for PO_4 adsorbed to Fe(III) (hydr)oxides. Hence, the color was assumed to give a more accurate representation of the P speciation in this Pt. Similarly, the major phase of Pt no. 5 of Skogaby 30–40 cm was determined to be an Fe-associated P phase, rather than Al-P, as shown by LCF. In this case, the XANES spectrum had a clear pre-edge (consistent with the µ-XRF color) but was of poor quality in the post-edge region, which might have caused LCF to produce the “wrong” result. For the remaining seven Pts, the spectral quality was not sufficient to support either interpretation, and hence the major P phase was considered undecided (Tables 1 and 2).

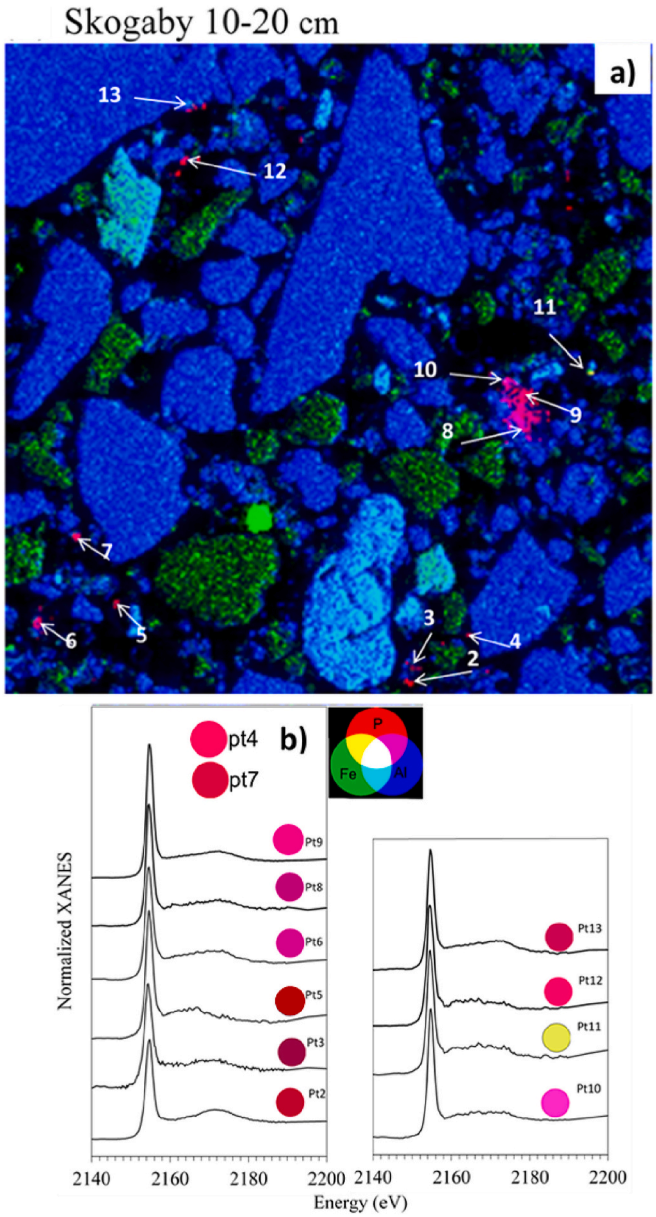

Fig. 4. RGB P-Fe-Al µ-XRF map (700 × 700 µm) of Skogaby 10–20 cm (B horizon) and corresponding normalized P K-edge µ-XANES spectra of µ-Pts, with the corresponding RGB colors as indicated by the color picker tool in the Affinity Designer software. The µ-XANES spectra of Pt 4 and Pt 7 are not shown due to their poor quality (for the spectra, see Fig. S3).

For the Flakaliden B horizon, there was a predominance of Al-P in both the 20–30 cm and 40–50 cm samples (Table 1). Of the 27 Pts in which the major phase was identified, Al-P dominated in 25. The strong intensity of the white line (i.e., the sharp peak at the top of the absorption edge; Figs. 3b and 5c) was consistent with a dominant role of adsorbed PO_4 (Gustafsson et al., 2020; Hesterberg et al., 2017; Yamaguchi et al., 2021). The ITM-adsorbed PO_4 standard appeared most frequently as a major P fraction in most LC fits, consistent with the FTIR and oxalate extraction results, showing ITM to be an important secondary Al phase in the soils. In the two remaining Pts (no. 3 of 20–30 cm, and no. 6 of 40–50 cm), Ca phosphates (Ca-P) dominated. In these Pts, the quality of the LCF, indicated by the relatively high value of the R-factor (Table 1), was poor, which was probably impacted by the locally very high concentrations of P, leading to self-absorption, and maybe also by the crystallinity of the particles. Moreover, as Fig. 3 and Fig. 5 show, the Pts were most commonly associated with Al-bearing particles. Overall, the results agree with the bulk XANES results from the same samples shown elsewhere, which showed 83% and 68% Al-P in the 20–30 and 40–50 cm samples, respectively (Table S2; Tuyishime et al., 2022). However, in the current study, we were also able to identify Ca-P, most likely in one Pt of the 20–30 sample; this species did not enter the bulk XANES-LCF of Tuyishime et al. (2022).

For the upper B horizon of Skogaby (10–20 cm), the results were somewhat more diverse (Table 2). Still, Al-P dominated in five out of nine Pts where the major phase could be determined. In two Pts, Ca-P (probably apatite) dominated, whereas organic P and Fe-P were major phases in one Pt each. Finally, for the lower B horizon (30–40 cm), Al-P was the major phase in nine of 11 Pts, with Fe-P and Ca-P being the major phases in one Pt each. Similar to the Flakaliden samples, the Pts in which Ca-P dominated were characterized by poor LC fits (i.e., high R factors) of P K-edge µ-XANES, although the general features of the XANES spectra were consistent with Ca-P, e.g., apatite. Again, this was probably due to the locally very high P concentrations of the micrometer-sized apatite grains and the associated self-absorption effects, some of which can be seen in Figs. S7-S10.

The B horizons of the two soil profiles studied differed considerably regarding organic P (P_{org}). For example, in the upper Skogaby B horizon (10–20 cm), µ-XANES-LCF identified P_{org} as between 3 and 43% of total P in eight (2, 3, 5, 6, 7, 8, 11, and 12) out of 12 Pts. However, P_{org} was nearly undetectable in microsites from the other three soil samples (Tables 1 and 2), consistent with their lower organic C contents (Table S1). The XANES spectrum of adsorbed P_{org} presents an intermediate shape between P_{org} and PO_4 adsorbed to Al/Fe (hydr)oxides (Gustafsson et al., 2020; Prietzel et al., 2016b). Thus, P K-edge XANES is not ideally suited for distinguishing between ‘free’ P_{org} and P_{org} adsorbed to Al and Fe minerals. Further, some Al- or Fe-adsorbed P_{org} may be incorrectly assigned as adsorbed inorganic PO_4 (Gustafsson et al., 2020; Prietzel et al., 2016b). Oxalate-extracted P fractions may provide a clue to the identity of the adsorbed P phases. On average, the P_{org} fraction of the sum of oxalate-extractable P was 12% in the Flakaliden B horizon, while it was 40% for the Skogaby B horizon (Tuyishime et al., 2022). This suggests that a considerable part of the adsorbed P at Skogaby may

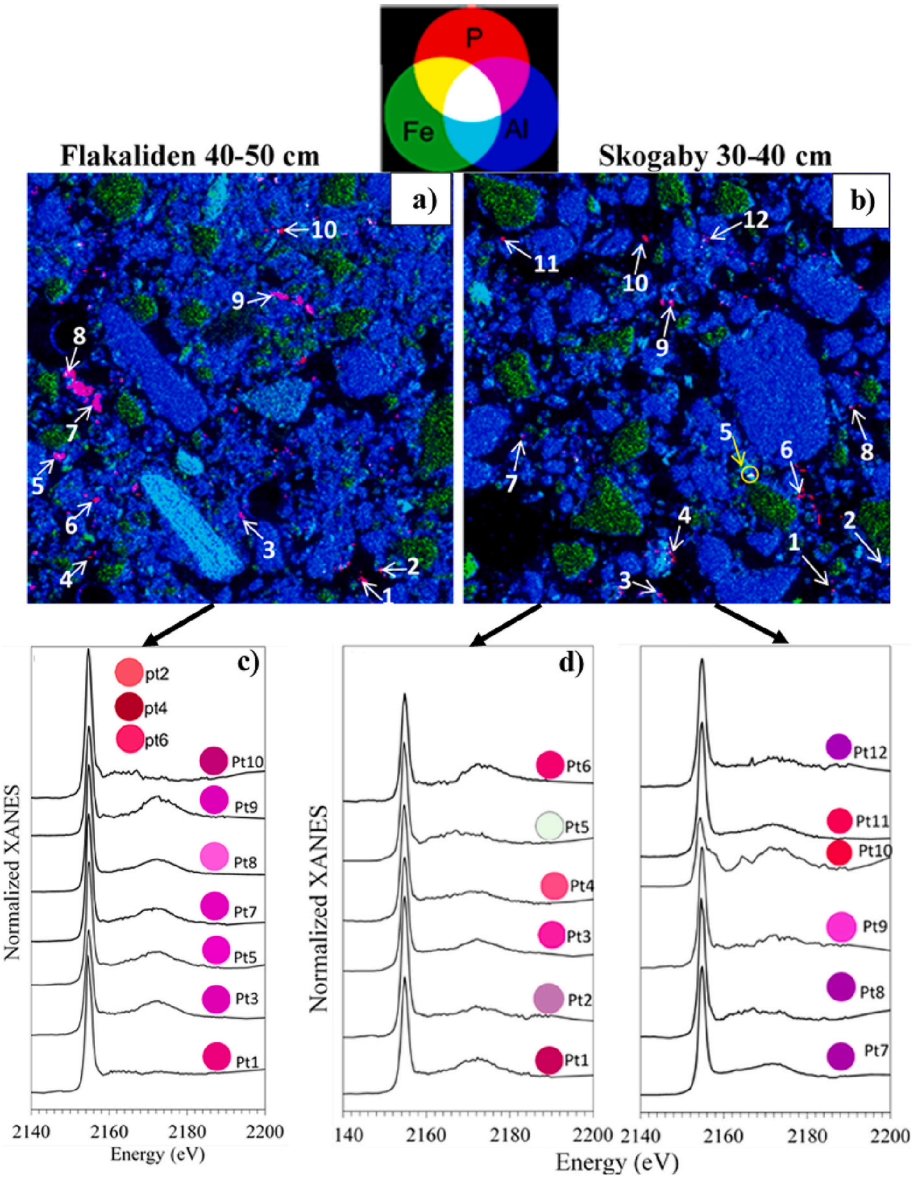

Fig. 5. RGB P-Fe-Al µ-XRF maps (700 × 700 µm) of a) Flakaliden 40–50 cm and b) Skogaby 30–40 cm, and corresponding normalized P K-edge µ-XANES spectra of µ-SPI of c) Flakaliden 40–50 cm, and d) and e) Skogaby 30–40 cm, with the corresponding RGB colors as indicated by the color picker tool in the Affinity Designer software.

be present as adsorbed P_{org}, while for Flakaliden, inorganic PO_4 very probably dominates the pool of adsorbed P species, in accordance with the XANES-LCF result.

In a previous study, it was hypothesized that the spatial distribution of Fe-P and Al-P species was more heterogeneous in the upper B horizon, as Fe oxides and ITM may have been formed from weathering in situ, while in the lower B, these precipitates had, to a larger extent, accumulated after migration of Fe- and Al-organic complexes from above horizons, resulting in mixing of the weathered Al and Fe and consequently to less spatial variation of the adsorbed P speciation (Adediran et al., 2020). This hypothesis was based on the microscale P speciation results of one of the two podzolised soils studied (Tärnsjö). The hypothesis is also consistent with the traditional view on the podzolization process, where the emphasis is on the migration of organic acids from the O and across the E horizon, organic complexation of weathered Fe and Al at the E-B horizon interface or in the upper B, and subsequent precipitation of the inorganic weathering products deeper down in the B horizon (Lundström et al., 2000). In principle, the heterogeneous distribution of Al-P vs. Fe-P can be estimated from the standard deviation of the ratio of Al-P to the sum of Al-P and Fe-P. For Skogaby 10–20 cm, this value was 0.38, showing a relatively large spatial variability in Al-P over Fe-P, whereas for Skogaby 30–40 cm, it was 0.24. However, in the Flakaliden soil, the standard deviation of the Al-P/(Al-P + Fe-P) ratio was 0.19 and 0.39 for the 20–30 and 40–50 cm layers respectively, hence showing a larger spatial variability of the deeper 40–50 cm sample. In other words, the hypothesis was consistent with the results for Skogaby, but not for Flakaliden. Hence it seems likely that the factors governing the spatial variability of the Al- and Fe-associated P species are more complex than the hypothesis of Adediran et al. (2020) would suggest.

The finding that the P elemental associations, as determined by µ-XRF, agree with the P speciation as determined by µ-XANES in the vast majority of cases, strengthens the conclusion that Al-associated P phases, consisting mostly of ITM-adsorbed PO_4 and to a lesser extent of ITM-bound organic P, dominate the P inventory of the B horizons of these and probably many other Podzols in boreal and hemiboreal climates. The significance of this finding concerning the bioavailability of P in forest ecosystems remains uncertain, although it has been remarked that ITMtype phases are less thermodynamically stable and more easily dissolved than Fe oxides, which could facilitate P acquisition by ectomycorrhizal fungi (e.g. Tuyishime et al., 2022).

4. Conclusion

This work reinforces earlier evidence that Al-associated P phases dominate the P inventory of the B horizon of Podzols. The Al-P consists mainly of inorganic PO_4 adsorbed to ITM and to a lesser degree of $AlPO_4$, although P_{org} adsorbed to Al phases may play an additional role, particularly in organic matter-rich B horizons. Fe-P (mainly as PO_4 or P_{org} adsorbed to Fe oxide and as $FePO_4$) is quantitatively less important for the studied horizons. However, on a microscale, it may be predominant in certain spots – particularly in the upper B horizon. Finally, Ca-P has a very heterogeneous spatial distribution and occurs concentrated in small spots, probably as unweathered apatite grains or inclusions, as has been discussed earlier (Adediran et al., 2020; Adediran et al., 2022).

In 45 of 54 cases (i.e., 83%), the color, as determined from the RGB µ-XRF maps, was consistent with the main P species determined using LCF of µ-XANES spectra. This shows that in most cases, it is possible to estimate the main P species only by µ-XRF when the associated elements of interest (in this case Al and Fe) are also mapped. Moreover, by combining information from µ-XRF with µ-XANES, the major P-containing species in a certain spot can be better constrained.

CRediT authorship contribution statement

J.R. Marius Tuyishime: Writing – review & editing, Writing – original draft, Visualization, Validation, Software, Methodology, Investigation, Formal analysis, Conceptualization. **Tove Florén:** Writing – review & editing, Writing – original draft, Methodology, Investigation. **Camille Rivard:** Writing – review & editing, Writing – original draft, Supervision, Software, Methodology, Investigation. **Jon Petter Gustafsson:** Writing – review & editing, Writing – original draft, Supervision, Resources, Funding acquisition, Conceptualization.

Declaration of competing interest

The authors declare that they have no known competing financial interests or personal relationships that could have appeared to influence the work reported in this paper.

Data availability

Data will be made available on request.

Acknowledgment

The authors would like to acknowledge the Swedish Research Council Formas for funding the work, grant number 2017-01139. Furthermore, we acknowledge the technical support at the LUCIA beamline at the French National Synchrotron Research Center SOLEIL (proposal n° 20210607). We thank Gulaim Seisenbaeva at the Swedish University of Agicultural Sciences for assistance with FTIR analysis. The authors also acknowledge Gbotemi Adediran at the U.K. Centre for Ecology and Hydrology and Carin Sjöstedt at the Swedish University of Agricultural Sciences for their support and discussions during µ-XRF data analysis and valuable comments on the manuscript.

Appendix A. Supplementary data

Supplementary data to this article can be found online at https://doi.org/10.1016/j.chemgeo.2024.122083.

References

Adediran, G.A., Tuyishime, J.M., Vantelon, D., Klysubun, W., Gustafsson, J.P., 2020. Phosphorus in 2D: spatially resolved P speciation in two Swedish forest soils as influenced by apatite weathering and podzolization. Geoderma 376, 114550. https://doi.org/10.1016/j.geoderma.2020.114550.

Adediran, G.A., Kielman-Schmitt, M., Kooijman, E., Gustafsson, J.P., 2022. Significance of phosphorus inclusions and discrete micron-sized grains of apatite in postglacial forest soils. Eur. J. Soil Sci. 73, e13310 https://doi.org/10.1111/ejss.13310.

Albaugh, T.J., Bergh, J., Lundmark, T., Nilsson, U., Stape, J.L., Allen, H.L., Linder, S., 2009. Do biological expansion factors adequately estimate stand-scale aboveground component biomass for Norway spruce? For. Ecol. Manag. 258, 2628–2637. https://doi.org/10.1016/j.foreco.2009.09.021.

Amadou, I., Faucon, M.-P., Houben, D., 2022. Role of soil minerals on organic phosphorus availability and phosphorus uptake by plants. Geoderma 428, 116125. https://doi.org/10.1016/j.geoderma.2022.116125.

Anderson, G., Williams, E.G., Moir, J.O., 1974. A comparison of the sorption of inorganic orthophosphate and inositol hexaphosphate by six acid soils. J. Soil Sci. 25, 51–62. https://doi.org/10.1111/j.1365-2389.1974.tb01102.x.

Beauchemin, S., Hesterberg, D., Chou, J., Beauchemin, M., Simard, R.R., Sayers, D.E., 2003. Speciation of phosphorus in phosphorus-enriched agricultural soils using X-ray absorption near-edge structure spectroscopy and chemical fractionation. J. Environ. Qual. 32, 1809–1819. https://doi.org/10.2134/jeq2003.1809.

Bergh, J., Linder, S., Lundmark, T., Elfving, B., 1999. The effect of water and nutrient availability on the productivity of Norway spruce in northern and southern Sweden. Forest Ecol. Manag. 119, 51–62. https://doi.org/10.1016/S0378-1127(98)00509-X.

Bergholm, J., Berggren, D., Alavi, G., 2003. Soil acidification induced by ammonium sulphate addition in a Norway spruce forest in Southwest Sweden. Water Air Soil Pollut. 148, 87–109.

Bishop, J.L., Ethbrampe, E.B., Bish, D.L., Abidin, Z.L., Baker, L.L., Matsue, N., Henmi, T., 2013. Spectral and hydration properties of allophane and imogolite. Clay Clay Miner. 61, 57–74. https://doi.org/10.1346/CCMN.2013.0610105.

Borggaard, O.K., Jørgensen, S.S., Møberg, J., Raben-Lange, B., 1990. Influence of organic matter on phosphate adsorption by aluminium and iron oxides in sandy soils. J. Soil Sci. 41, 443–449. https://doi.org/10.1111/j.1365-2389.1990.tb00078.x.

Borggaard, O.K., Szilas, C., Gimsing, A.L., Rasmussen, L.H., 2004. Estimation of soil phosphate adsorption capacity by means of a pedotransfer function. Geoderma 118, 55–61. https://doi.org/10.1016/S0016-7061(03)00183-6.

Buurman, P., van Reeuwijk, L., 1984. Proto-imogolite and the process of podzol formation: a critical note. J. Soil Sci. 35, 447–452. https://doi.org/10.1111/j.1365-2389.1984.tb00301.x.

Casetou-Gustafson, S., Hillier, S., Akselsson, C., Simonsson, M., Stendahl, J., Olsson, B.A., 2018. Comparison of measured (XRPD) and modeled (A2M) soil mineralogies: a study of some Swedish forest soils in the context of weathering rate predictions. Geoderma 310, 77–88. https://doi.org/10.1016/j.geoderma.2017.09.004.

Casetou-Gustafson, S., Akselsson, C., Hillier, S., Olsson, B.A., 2019. The importance of mineral determinations to PROFILE base cation weathering release rates: a case study. Biogeosciences 16, 1903–1920. https://doi.org/10.5194/bg-16-1903-2019.

Casetou-Gustafson, S., Grip, H., Hillier, S., Linder, S., Olsson, B.A., Simonsson, M., Stendahl, J., 2020. Current, steady-state and historical weathering rates of base cations at two forest sites in northern and southern Sweden: a comparison of three methods. Biogeosciences 17, 281–304. https://doi.org/10.5194/bg-17-281-2020.

Chandez, F., Montarou, G., 2010. Analyse Avec le Logiciel ImageJ d'un lot d'images en Microscopie par Immunofluorecence de Cellules de Fibroblastes Irradiées en X à l'ESRF, p. 71. https://hal.in2p3.fr/in2p3-00530281. Last accessed: 2023-08-08.

Doydora, S., Gatiboni, L., Grieger, K., Hesterberg, D., Jones, J.L., McLamore, E.S., Peters, R., Sozzani, R., Van den Broeck, L., Duckworth, O.W., 2020. Accessing legacy phosphorus in soils. Soil Syst. 4, 74. https://doi.org/10.3390/soilsystems4040074.

Eriksson, A.K., Hillier, S., Hesterberg, D., Klysubun, W., Ulén, B., Gustafsson, J.P., 2016. Evolution of phosphorus speciation with depth in an agricultural soil profile. Geoderma 280, 29–37. https://doi.org/10.1016/j.geoderma.2016.06.004.

Farmer, V.C., Fraser, A.R., Russell, J.D., Yoshinaga, N., 1977. Recognition of imogolite structures in allophanic clays by infrared spectroscopy. Clay Miner. 12, 55–57. https://doi.org/10.1180/claymin.1977.012.1.04.

Farmer, V.C., Russell, J.D., Berrow, M.L., 1980. Imogolite and proto-imogolite allophane in spodic horizons: evidence for a mobile aluminium silicate complex in podzol formation. J. Soil Sci. 31, 673–684. https://doi.org/10.1111/j.1365-2389.1980.tb02113.x.

Gustafsson, J.P., Bhattacharya, P., Bain, D.C., Fraser, A.R., McHardy, W.J., 1995. Podzolisation mechanisms and the synthesis of imogolite in northern Scandinavia. Geoderma 66, 167–184. https://doi.org/10.1016/0016-7061(95)00005-9.

Gustafsson, J.P., Bhattacharya, P., Karltun, E., 1999. Mineralogy of poorly crystalline aluminium phases in the B horizon of Podzols in southern Sweden. Appl. Geochem. 14, 707–718. https://doi.org/10.1016/S0883-2927(99)00002-5.

Gustafsson, J.P., Braun, S., Tuyishime, J.R.M., Adediran, G.A., Warrinnier, R., Hesterberg, D., 2020. A probabilistic approach to phosphorus speciation of soils using P K-edge XANES spectroscopy with linear combination fitting. Soil Syst. 4, 26. https://doi.org/10.3390/soilsystems4020026.

Hesterberg, D., 2010. Macroscale chemical properties and X-ray absorption spectroscopy of soil phosphorus. Dev. Soil Sci. 34, 313–356. https://doi.org/10.1016/S0166-2481(10)34011-6.

Hesterberg, D., Duff, M.C., Dixon, J.B., Vepraskas, M.J., 2011. X-ray microspectroscopy and chemical reactions in soil microsites. J. Environ. Qual. 40, 667–678. https://doi.org/10.2134/jeq2010.0140.

Hesterberg, D., McNulty, I., Thieme, J., 2017. Speciation of soil phosphorus assessed by XANES spectroscopy at different spatial scales. J. Environ. Qual. 46, 1190–1197. https://doi.org/10.2134/jeq2016.11.0431.

IUSS Working Group, 2014. World Reference Base for Soil Resources. International Soil Classification System for Naming Soils and Creating Legends for Soil Maps. World Soil Resources Reports no. 106. FAO, Rome, Italy.

Klotzbücher, A., Schunck, F., Klotzbücher, T., Kaiser, K., Glaser, B., Spohn, M., Widdig, M., Mikutta, R., 2020. Goethite-associated phosphorus is not available to beech (*Fagus sylvatica* L.). Front. For. Glob. Change 3, 94. https://doi.org/10.3389/ffgc.2020.00094.

Lang, F., Krüger, J., Amelung, W., Willbold, S., Frossard, E., Bünemann, E.K., Bauhus, J., Nitschke, R., Kandeler, E., Marhan, S., Schulz, S., Bergkemper, F., Schloter, M., Luster, J., Guggisberg, F., Kaiser, K., Mikutta, R., Guggenberger, G., Polle, A., Pena, R., Prietzel, J., Rodionov, A., Talkner, U., Meesenburg, H., von Wilpert, K., Hölscher, A., Dietrich, H.P., Chamara, I., 2017. Soil phosphorus supply controls P nutrition strategies of beech forest ecosystems in Central Europe. Biogeochemistry 136, 5–29. https://doi.org/10.1007/s10533-017-0375-0.

Lundström, U.S., van Breemen, N., Bain, D.C., van Hees, P.A.W., Giesler, R., Gustafsson, J.P., Ilvesniemi, H., Karltun, E., Melkerud, P.-A., Olsson, M., Riise, G., Wahlberg, O., Bergelin, A., Bishop, K., Finlay, R., Jongmans, A.G., Magnusson, T., Mannerkoski, H., Nordgren, A., Nyberg, L., Starr, M., Strand, L.T., 2000. Advances in understanding the podzolization process resulting from a multidisciplinary study of three coniferous forest soils in the Nordic Countries. Geoderma 94, 335–353. https://doi.org/10.1016/S0016-7061(99)00077-4.

Nilsson, L.-O., Wiklund, K., 1995. Indirect effects of N and S deposition on a Norway spruce ecosystem. An update of findings within the Skogaby project. Water Air Soil Pollut. 85, 1613–1622.

Parfitt, R.L., 1979. The nature of the phosphate-goethite (α-FeOOH) complex formed with ca$(H_2PO_4)_2$ at different surface coverage. Soil Sci. Soc. Am. J. 43, 623–625. https://doi.org/10.2136/sssaj1979.03615995004300030039x.

Parfitt, R.L., 1989. Phosphate reactions with natural allophane, ferrihydrite and goethite. J. Soil Sci. 40, 359–369. https://doi.org/10.1111/j.1365-2389.1989.tb01280.x.

Prietzel, J., Klysubun, W., Werner, F., 2016a. Speciation of phosphorus in temperate zone forest soils as assessed by combined wet-chemical fractionation and XANES spectroscopy. J. Plant Nutr. Soil Sci. 179, 168–185. https://doi.org/10.1002/jpln.201500472.

Prietzel, J., Harrington, G., Häusler, W., Heister, K., Werner, F., Klysubun, W., 2016b. Reference spectra of important adsorbed organic and inorganic phosphate binding forms for soil P speciation using synchrotron-based K-edge XANES spectroscopy. J. Synchrotron Radiat. 23, 532–544. https://doi.org/10.1107/S1600577515023085.

Prietzel, J., Krüger, J., Kaiser, K., Amelung, W., Bauke, S.L., Dippold, M.A., Kandeler, E., Klysubun, W., Lewandowski, H., Löppmann, S., 2022. Soil phosphorus status and P nutrition strategies of European beech forests on carbonate compared to silicate parent material. Biogeochemistry 158, 39–72. https://doi.org/10.1007/s10533-021-00884-7.

Ravel, B., 2009. ATHENA - A User's Guide. Web. https://bruceravel.github.io/demeter/aug/. Last accessed: 2023-08-08.

Ravel, B., Newville, M., 2005. Athena, artemis, hephaestus: data analysis for X-ray absorption spectroscopy using Ifeffit. J. Synchrotron Radiat. 12, 537–541. https://doi.org/10.1107/S0909049505012719.

Richardson, A.E., Simpson, R.J., 2011. Soil microorganisms mediating phosphorus availability. Update on microbial phosphorus. Plant Physiol. 156, 989–996. https://doi.org/10.1104/pp.111.175448.

Rivard, C., Lanson, B., Cotte, M., 2016. Phosphorus speciation and micro-scale spatial distribution in North-American temperate agricultural soils from micro X-ray fluorescence and X-ray absorption near-edge spectroscopy. Plant Soil 401, 7–22. https://doi.org/10.1007/s11104-015-2494-5.

Sauer, D., Sponagel, H., Sommer, M., Giani, L., Jahn, R., Stahr, K., 2007. Podzol: Soil of the year 2007. A review on its genesis, occurrence, and functions. J. Plant Nutr. Soil Sci. 170, 581–597. https://doi.org/10.1002/jpln.200700135.

Schreider, K., Hofmann, D., Boy, D., Andrino, A., Figueiredo, A.F., Sauheitl, L., Guggenberger, G., 2022. Mycorrhizal mediated partitioning of phosphorus: ectomycorrhizal (*Populus* × *canescens* × *Paxillus involutus*) potential to exploit simultaneously organic and mineral phosphorus sources. Front. Soil Sci. 2, 865517 https://doi.org/10.3389/fsoil.2022.865517.

Simonsson, M., Bergholm, J., Olsson, B.A., von Brömssen, C., Öborn, I., 2015. Estimating weathering rates using base cation budgets in a Norway spruce stand on podzolised soil: analysis of fluxes and uncertainties. Forest Ecol. Manag. 340, 135–152. https://doi.org/10.1016/j.foreco.2014.12.024.

Simonsson, M., Court, M., Bergholm, J., Lemarchand, D., Hillier, S., 2016. Mineralogy and biogeochemistry of potassium in the Skogaby experimental forest, Southwest Sweden: pools, fluxes and K/Rb ratios in soil and biomass. Biogeochemistry 131, 77–102. https://doi.org/10.1007/s10533-016-0266-9.

Solé, V.A., Papillon, E., Cotte, M., Walter, P., Susini, J., 2007. A multiplatform code for the analysis of energy-dispersive X-ray fluorescence spectra. Spectrochim. Acta B 62, 63–68. https://doi.org/10.1016/j.sab.2006.12.002.

Tuyishime, J.R.M., Adediran, G.A., Olsson, B.A., Spohn, M., Hillier, S., Klysubun, W., Gustafsson, J.P., 2022. Phosphorus abundance and speciation in acid forest Podzols - effect of postglacial weathering. Geoderma 406, 115500. https://doi.org/10.1016/j.geoderma.2021.115500.

van der Bom, F.J.T., Kopittke, P.M., Raymond, N.S., Sekine, R., Lombi, E., Mueller, C.W., Doolette, C.L., 2022. Methods for assessing laterally-resolved distribution, speciation and bioavailability of phosphorus in soils. Rev. Environ. Sci. Biotechnol. 21, 53–74. https://doi.org/10.1007/s11157-021-09602-z.

Vantelon, D., Trcera, N., Roy, D., Moreno, T., Mailly, D., Guilet, S., Metchalkov, E., Delmotte, F., Lassalle, B., Lagarde, P., Flanck, A.-M., 2016. The LUCIA beamline at SOLEIL. J. Synchrotron Radiat. 23, 635–640. https://doi.org/10.1107/S1600577516000746.

Vitousek, P.M., Porder, S., Houlton, B.Z., Chadwick, O.A., 2010. Terrestrial phosphorus limitation: mechanisms, implications, and nitrogen–phosphorus interactions. Ecol. Appl. 20, 5–15. https://doi.org/10.1890/08-0127.1.

Vogel, C., Helfenstein, J., Massey, M.S., Sekine, R., Kretzschmar, R., Beiping, L., Peter, T., Chadwick, O.A., Tamburini, F., Rivard, C., Herzel, H., Adam, C., Pradas del Real, A. E., Castillo-Michel, H., Zuin, L., Wang, D., Félix, R., Lassalle-Kaiser, B., Frossard, E., 2021. Microspectroscopy reveals dust-derived apatite grains in acidic, highly-weathered Hawaiian soils. Geoderma 381, 114681. https://doi.org/10.1016/j.geoderma.2020.114681.

Wood, T., Bormann, F.H., Voigt, G.K., 1984. Phosphorus cycling in a northern hardwood forest: biological and chemical control. Science 223, 391–393. https://doi.org/10.1126/science.223.4634.391.

Yamaguchi, N., Ohkura, T., Hikono, A., Hashimoto, Y., Suda, A., Yamamoto, T., Ando, K., Kasuya, M., Northrup, P., Wang, S.-L., Hesterberg, D., 2021. Microscale heterogeneous distribution and speciation of phosphorus in soils amended with mineral fertilizer and cattle manure compost. Minerals 11, 121. https://doi.org/10.3390/min11020121.